Theory of Swimming Filaments in Viscoelastic Media

Henry C. Fu and Thomas R. Powers

Division of Engineering, Brown University, Providence, Rhode Island 02912, USA

Charles W. Wolgemuth

Department of Cell Biology, University of Connecticut Health Center, Farmington, Connecticut 06030, USA
(Received 30 July 2007; published 19 December 2007)

Motivated by our desire to understand the biophysical mechanisms underlying the swimming of sperm in the non-Newtonian fluids of the female mammalian reproductive tract, we examine the swimming of filaments in the nonlinear viscoelastic upper convected Maxwell model. We obtain the swimming velocity and hydrodynamic force exerted on an infinitely long cylinder with prescribed beating pattern. We use these results to examine the swimming of a simplified sliding-filament model for a sperm flagellum. Viscoelasticity tends to decrease swimming speed, and changes in the beating patterns due to viscoelasticity can reverse swimming direction.

PACS numbers: 87.19.St, 47.15.Gf, 87.16.Qp

The physical environment of the cell places severe constraints on mechanisms for motility. For example, viscous effects dominate inertial effects in water at the scale of a few microns. Therefore, swimming cells use viscous resistance to move, since mechanisms that rely on imparting momentum to the surrounding fluid, such as waving a rigid oar, do not work [1,2]. The fundamental principles of swimming in the low-Reynolds number regime of small-scale, slow flows have been established for many years [2–5], yet continue to be an area of active research. However, when a sperm cell moves through the viscoelastic mucus of the female mammalian reproductive tract, the theory of swimming in a purely viscous fluid is inapplicable. Observations of sperm show that they are strongly affected by differences between viscoelastic and viscous fluids. In particular, the shape of the flagellar beating pattern as well as swimming trajectories and velocities depend on the properties of the medium [6–8].

The interplay of medium properties and flagellar motility or transport also arises in other situations, such as spirochetes swimming in a gel [9], and cilia beating in mucus to clear foreign particles in the human airway [10]. Motivated by these phenomena, we develop a theory for swimming filaments in a viscoelastic medium. To leading order in the amplitude of the deflection of the filament, there are two corrections to the swimming velocity when the medium changes from Newtonian to non-Newtonian. The first depends only on the properties of the medium, and we elucidate it by analyzing an infinite filament with a prescribed beating pattern in a fluid described by the upper convected Maxwell (UCM) model [11]. Our results extend the findings of Lauga [12], who considered a variety of fading memory models for the case of a prescribed beat pattern on a planar sheet. The second correction to the swimming speed arises because the nature of the medium affects the beating pattern of a filament. We elucidate this effect using a simple model flagellum with active internal forces.

Newtonian fluids are characterized by a simple constitutive relation, in which stress is proportional to strain rate. Non-Newtonian fluids cannot be characterized by a simple universal constitutive relation, and exhibit a range of phenomena such as elasticity, shear thinning, and yield stress behavior. We choose to focus our attention on fluids with fading memory, in which the stress relaxes over time to the viscous stress. We consider small-amplitude deflections of an infinite filament of radius a (Fig. 1). Since the swimming velocity of a filament is second order in the deflection amplitude [3,4], linear models for fading memory such as the Maxwell model are insufficient for studying swimming [12]. Therefore, we use a simple nonlinear constitutive relation incorporating elastic effects, the UCM model. This model is appropriate for a polymer solution in which the viscosity of the Newtonian solvent is disregarded:

$$\boldsymbol{\tau} + \lambda \hat{\boldsymbol{\tau}} = \eta \dot{\boldsymbol{\gamma}}. \qquad (1)$$

In this equation $\boldsymbol{\tau}$ is the deviatoric stress, λ is the relaxation time, $\hat{\boldsymbol{\tau}} = \partial_t \boldsymbol{\tau} + \mathbf{v} \cdot \nabla \boldsymbol{\tau} - (\nabla \mathbf{v})^{\mathsf{T}} \cdot \boldsymbol{\tau} - \boldsymbol{\tau} \cdot \nabla \mathbf{v}$ is the upper-convected time derivative of $\boldsymbol{\tau}$, $\mathbf{v}$ is the velocity, η is the polymer viscosity, and $\dot{\boldsymbol{\gamma}} = \nabla \mathbf{v} + (\nabla \mathbf{v})^{\mathsf{T}}$ is the strain rate. The nonlinear terms of the upper-convected derivative make the constitutive relation insensitive to translational and rotational motion of material elements [11]. The UCM fluid responds as an elastic solid when subject to a rapidly
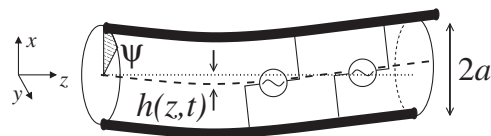

FIG. 1. Cylinder with imposed traveling-wave transverse displacement. The dark lines indicate filaments in the active flagellum model. The active elements inside the flagellum represent motors that slide the filaments relative to each other.

varying stress, and as a viscous liquid when subject to a slowly varying stress. When $\lambda = 0$, the constitutive relation (1) is Newtonian. Since inertia is unimportant, the motion of the medium is governed by force balance, $-\nabla p + \nabla \cdot \boldsymbol{\tau} = 0$, or

$$- (1 + \lambda \partial_t)\nabla p + \eta \nabla^2 \mathbf{v} = \lambda \nabla \cdot \mathbf{T}, \tag{2}$$

where $\mathbf{T} = \mathbf{v} \cdot \nabla \boldsymbol{\tau} - (\nabla \mathbf{v})^{\mathsf{T}} \cdot \boldsymbol{\tau} - \boldsymbol{\tau} \cdot \nabla \mathbf{v}$, and we have assumed incompressibility, $\nabla \cdot \mathbf{v} = 0$.

To calculate the swimming velocity of the filament, we prescribe a beating pattern that is independent of load, and solve (2) for the flow, imposing no-slip boundary conditions at the filament surface. Material points on the filament surface are parameterized by z and ψ (see Fig. 1), and are given by

$$\mathbf{r}(z, \psi, t) = [h(z, t) + a\cos(\psi)]\hat{\mathbf{x}} + a\sin(\psi)\hat{\mathbf{y}} + z\hat{\mathbf{z}}, \tag{3}$$

where $h(z, t) = \mathrm{Re}\sum_{q,\omega} h_{q\omega} \exp(iqz - i\omega t)$. Note that we work in the frame in which material points of the cylinder move in planes of constant z. We will find that the no-slip boundary conditions can only be satisfied if there is a uniform flow along the z axis. In the lab frame in which the fluid is at rest at infinity, the flow corresponds to the swimming velocity of the cylinder.

Invoking small amplitude, long wavelength distortions for simplicity, we solve the equations order by order in the displacement amplitudes $qh_{q\omega}$, to lowest order in $1/\log qa$, and assuming that $h_{q\omega}/a \ll 1$. Expressing the dynamic variables as expansions in $qh_{q\omega}$, such as $\mathbf{v} = \mathbf{v}^{(1)} + \mathbf{v}^{(2)} + \ldots$, the no-slip boundary condition $\dot{h}(z, t)\hat{\mathbf{x}} = \mathbf{v}[\mathbf{r}(z, \psi, t)]$ up to second order is

$$\dot{h}\,\hat{\mathbf{x}} = \mathbf{v}^{(1)} + \mathbf{v}^{(2)} + h(\cos\psi\,\hat{\mathbf{r}} - \sin\psi\,\hat{\boldsymbol{\phi}}) \cdot \nabla\mathbf{v}^{(1)}, \tag{4}$$

where h is evaluated at (z, t), and $\mathbf{v}$, $\hat{\mathbf{r}}$, and $\hat{\boldsymbol{\phi}}$ at cylindrical coordinates (a, ψ, z, t). We used the fact that the material point labeled ψ on the cylinder surface has coordinates $(\phi, r, z) \approx (\psi - (h/a)\sin\psi, a + h\cos\psi, z)$. There is no first order contribution to $\mathbf{T}$ and the first order dynamical equations are

$$(1 + \lambda\partial_t)\boldsymbol{\tau}^{(1)} = \eta\dot{\boldsymbol{\gamma}}^{(1)}, \tag{5}$$

$$(1 + \lambda\partial_t)\nabla p^{(1)} = \eta\nabla^2\mathbf{v}^{(1)}, \tag{6}$$

with $\nabla \cdot \mathbf{v}^{(1)} = 0$. Since Eq. (6) is the Stokes equation with a modified pressure, the solution is readily found [13], and the first order flow $\mathbf{v}^{(1)}$ is the same as in the purely viscous case in the limit $qa \ll 1$. The formulas for this flow are given by Taylor in [4]. Just as in Taylor's case, the swimming velocity vanishes to first order in $qh_{q\omega}$. Using the pressure and stress, we find that the force per unit length is purely in the $\hat{\mathbf{x}}$ direction:

$$\mathbf{f}^{(1)}_{\mathrm{fluid}}(z, t) = \mathrm{Re}\sum_{q,\omega} \frac{-4\pi\eta i\omega h_{q\omega}}{(1 - i\lambda\omega)\log qa} e^{iqz - i\omega t}\hat{\mathbf{x}}. \tag{7}$$

This is consistent with the results of Fulford, Katz, and Powell, who used resistive force theory for a filament in a linear Maxwell fluid, and found that for a prescribed beating pattern the swimming velocity is the same as in the viscous case, even to *second order* in $qh_{q\omega}$ [14].

In our problem, however, the nonlinearities make the viscoelastic swimming velocity different from the viscous swimming velocity. To second order,

$$(1 + \lambda\partial_t)\boldsymbol{\tau}^{(2)} = \eta\dot{\boldsymbol{\gamma}}^{(2)} - \lambda\mathbf{T}^{(2)}, \tag{8}$$

$$(1 + \lambda\partial_t)\nabla p^{(2)} = \eta\nabla^2\mathbf{v}^{(2)} - \lambda\nabla \cdot \mathbf{T}^{(2)}, \tag{9}$$

where $\mathbf{T}^{(2)}$ can be calculated using only the first order stresses and velocity fields. To find the time-averaged swimming velocity, we need only examine the velocity fields averaged over time and ϕ. To second order, we find that there is a uniform flow at infinity, corresponding to a swimming velocity in the lab frame of

$$\mathbf{U}^{(2)} = -\frac{1}{2}\sum_{q,\omega} \frac{|h_{q\omega}|^2 q\omega}{1 + (\lambda\omega)^2}\hat{\mathbf{z}}. \tag{10}$$

For a single traveling wave the direction of swimming is opposite the direction of motion of the traveling wave. Our result, valid to first order in $1/\log(qa)$, is the same as that for a traveling wave on a planar sheet [12].

We have dealt with the effects of viscoelasticity on a swimming filament with prescribed shape $h(z, t)$. In contrast, the beating patterns and the swimming velocity of real sperm are affected by the medium, suggesting that prescribing the shape changes of the swimmer may miss important effects. Therefore, we consider a sliding-filament model in which we prescribe active internal bending forces [15,16], and solve for flagellum shape as well as swimming speed. We continue to assume the flagellum has a cylindrical cross section and deflection $h\hat{\mathbf{x}}$, but now we assume the flagellum has finite length L and two inextensible longitudinal filaments with constant lateral spacing $2a$ (Fig. 1). Motors along the flagellum attach to both filaments and tend to slide them past each other. Sliding is prohibited at the end near the head, which is omitted for simplicity. Assuming a planar shape of the flagellum, the moment $\mathbf{M} = M\hat{\mathbf{y}}$ acting at a cross section of the flagellum consists of a passive resistance to bending, and an active part due to the sliding motors. To first order in deflection h,

$$M(z) = Ah'' - 2a\int_z^L f_m dz, \tag{11}$$

where A is the bending stiffness, primes denote derivatives with respect to z, and f_m is the force per unit length that the lower filament of Fig. 1 exerts on the upper filament. For simplicity we disregard any elastic or viscous effects arising from proteins linking the filaments.

The balance of internal forces and hydrodynamic forces determines the instantaneous shape of the flagellum [17,18]. To find the internal force per unit length f_{int}, consider moment balance on an element of the flagellum to first order in deflection [19]: $M' + N = 0$, where N is

the shear force acting on a cross section in the x direction. Using $f_{\text{int}} = N'$ yields $f_{\text{int}} = -Ah'''' - 2af'_m$. We choose a sliding force $f_m = \text{Re}[f\exp(ikz - i\omega t)]$. To linear order, the shape change occurs with only one frequency ω, and $h(z, t) = \text{Re}[\tilde{h}(z)\exp(-i\omega t)]$.

Since the internal forces f_{int} are expressed in real space, it is convenient to write the hydrodynamic force Eq. (7) in real space. The logarithm in Eq. (7) varies slowly with q and we replace it with a constant, $\log(qa) \approx \log(a/L)$, as is commonly done in resistive force theory. Thus

$$\mathbf{f}_{\text{fluid}} = \text{Re}\frac{-\zeta_\perp}{1 - i\lambda\omega}(-i\omega\tilde{h}(z)e^{-i\omega t})\hat{\mathbf{x}}, \qquad (12)$$

where $\zeta_\perp \approx 4\pi\eta/\log(L/a)$. It is sufficient to consider shape changes at linear order because the swimming speed is already second order in deflection. Note that although we use the same linear hydrodynamic force as Fulford, Katz, and Powell [14], they only consider one fixed waveform and do not allow beating patterns to respond to the change in hydrodynamic forces.

We nondimensionalize our equations of motion by measuring lengths in terms of L, f_m in terms of $A/(2aL^2)$, and time in terms of ω^{-1}. For notational simplicity, after scaling we use the same symbols for the new quantities. The equation of motion for the active flagellum is $\mathbf{f}_{\text{int}} + \mathbf{f}_{\text{fluid}} = 0$, or in nondimensional form,

$$\frac{-i\text{Sp}^4}{1 - i\text{De}}\tilde{h} + \tilde{h}'''' - ikf = 0. \qquad (13)$$

The dimensionless "sperm number" $\text{Sp} = L(\omega\zeta_\perp/A)^{1/4}$ is the fourth root of the ratio of the bending relaxation time of the flagellum to the period of the traveling wave, and the Deborah number $\text{De} = \lambda\omega$ measures the importance of elastic effects. Following [16], we estimate $L = 40~\mu\text{m}$, $a = 20~\text{nm}$, $A = 4 \times 10^{-22}~\text{N m}^2$, $\omega/(2\pi) = 30~\text{s}^{-1}$, and $\zeta_\perp = 2 \times 10^{-3}~\text{N s m}^{-2}$, and a dimensional magnitude of

internal sliding forces $f_m = 4~\text{pN}/(24~\text{nm})$. Therefore, $\text{Sp} \approx 7$, and the dimensionless amplitude $f \approx 13$. For sperm which oscillate at frequency 25–50 Hz in cervical mucus with time constant $\lambda \approx 1$–10 s [20], we take $\text{De} \approx 100$. Equation (13) must be supplemented by boundary conditions. For simplicity we forbid transverse motion of the head $h(0) = 0$, and suppose the connection between the head and the flagellum cannot support a moment: $h''(0) + \int_0^1 f_m(z)dz = 0$ (see [21] for a more realistic treatment of the moment boundary condition). The boundary condition at the other end is zero force, $-h'''(1) + f_m(1) = 0$, and zero moment, $h''(1) = 0$.

Representative plots of the beating patterns are shown in Fig. 2 (see supplementary material [22]). Two length scales are apparent. The first is the wavelength of the sliding force, $2\pi/k$, readily apparent in the change of beating patterns from $k = 0$ to $k = 8\pi/L$ at $\text{Sp} = 7$. The second length scale ξ arises from the interaction of bending and hydrodynamic forces: $\xi/L = |1 - i\text{De}|^{1/4}/\text{Sp}$. The flagellum behaves like a rigid rod for large ξ/L, and is floppy for small ξ/L. Changing the viscoelastic properties of the fluid affects the beating shapes through ξ (e.g., compare beating patterns for $\text{De} = 0$ and $\text{De} = 100$ in the flagellum with $k = 8\pi/L$ and $\text{Sp} = 7$). In Fig. 2, the amplitude of the sliding force is selected so that the maximum displacement of the flagellum is $L/10$. As De increases, ξ increases and so smaller driving forces are required. The beating pattern is linear in the driving force, so the results for constant driving force can be deduced from the forces provided in Fig. 2. Besides affecting ξ, viscoelasticity affects phase behavior: for $\text{De} = 0$, beating patterns are traveling waves, while for large De they are standing waves.

By inserting the beating pattern $h_{q\omega}$ into Eq. (10), we can calculate the swimming speed of a flagellum with prescribed internal forces. Although our flagellum is finite, we may apply Eq. (10) to our calculated beating pattern by
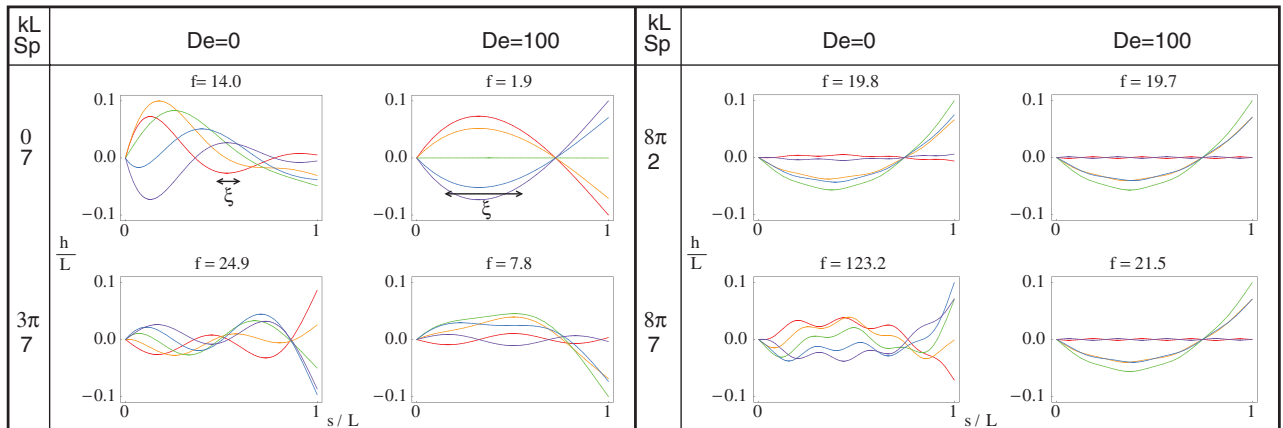

FIG. 2 (color).   Dimensionless amplitude h/L versus dimensionless arclength s/L for beating flagella with internal sliding forces. We show a half-cycle (red, orange, green, light blue, blue) of the pattern for viscous ($\text{De} = 0$) and viscoelastic ($\text{De} = 100$) cases. For $\text{Sp} = 7$, we show internal sliding forces with k varying from 0 (uniform force) to 8π. For $k = 8\pi/L$ we show the effect of varying sperm number. ξ is indicated on the $k = 0$ plots. The amplitude is linear in the driving force; at the top of each plot, we write the (dimensionless) magnitude f required to produce motion with amplitude $0.1L$.
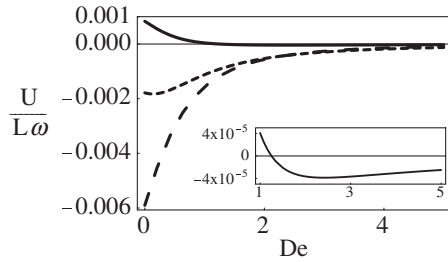
FIG. 3. Dimensionless swimming velocities versus De, for Sp = 7 for $k = 0$ (long dashes), $k = 3\pi/L$ (short dashes), $k = 8\pi/L$ (solid). For each wave vector, the magnitude of the driving force is chosen so that the maximum deflection amplitude at De = 0 is $0.1L$. Detail of the same plot (inset) shows that viscoelastic effects can reverse the swimming direction.

periodically replicating it to infinite extent in z. Physically, we are ignoring end effects. It is useful to rewrite Eq. (10) in real space, for an infinite flagellum with period L and single oscillation frequency ω:

$$\mathbf{U}^{(2)} = -\frac{1}{2L(1 + \mathrm{De}^2)} \int_0^L \langle \dot{h}(z, t) h'(z, t) \rangle dz \hat{\mathbf{z}}, \qquad (14)$$

where the dot denotes the time derivative and the brackets denote time averaging. The swimming velocity is independent of whether we consider the period L or nL; thus, the periodically replicated flagellum has the same velocity as the single flagellum, up to end effects.

The velocities of active flagella are plotted in Fig. 3. Viscoelastic effects can produce qualitative changes in the swimming velocity. Most notably, as De is increased, the velocity can change direction, for example, in the case of $k = 8\pi/L$. For De = 0, there is a small-amplitude traveling wave moving in the $+\hat{\mathbf{z}}$ direction with wavelength $\approx L/4$ driven by the sliding forces, but there is also a larger amplitude traveling wave moving in the $-\hat{\mathbf{z}}$ direction (Fig. 2). A filament swims in the opposite direction of the motion of its traveling waves, so these have opposing effects, but the net velocity is in the $+\hat{\mathbf{z}}$ direction. As De increases, the larger amplitude wave becomes a standing wave, and the remaining small-amplitude traveling waves move the flagellum in the $-\hat{\mathbf{z}}$ direction. We emphasize that this effect is not due to the $(1 + \mathrm{De}^2)$ correction of Eq. (14), which can never reverse the swimming direction. For swimming in viscoelastic fluids it is crucial to allow flagellum shapes to respond to changed forces rather than prescribe fixed beating patterns.

We conclude by indicating directions for future work. It is important to pursue numerical approaches to study the effects of free ends and large displacements. More realistic models for polymer solutions should also be explored, since the UCM model is invalid for sufficiently high extensional flows. A further extension of our work would be to consider swimming in a gel, which is a better model for mucus. Finally, it is important to determine if the internal

motor forces on the filaments are dependent on the load, as suggested by the fact that the beating frequency depends upon the medium [6–8]. An alternative experimental approach which sidesteps the uncertainty about internal workings of flagella would be to study magnetically driven artificial swimmers [23] in polymer solutions; our analysis can be easily adapted to this case.

[1] W. Ludwig, Z. Vgl. Physiol. **13**, 397 (1930).
[2] E. M. Purcell, Am. J. Phys. **45**, 3 (1977).
[3] G. I. Taylor, Proc. R. Soc. A **209**, 447 (1951).
[4] G. I. Taylor, Proc. R. Soc. A **211**, 225 (1952).
[5] J. Lighthill, SIAM Rev. **18**, 161 (1976).
[6] H. Ho and S. S. Suarez, Rep. Dom. Anim. **38**, 119 (2003).
[7] S. Suarez, D. Katz, D. Owen, J. Andrew, and R. Powell, Biol. Reprod. **44**, 375 (1991).
[8] S. Suarez and X. Dai, Biol. Reprod. **46**, 686 (1992).
[9] N. W. Charon and S. F. Goldstein, Annu. Rev. Genet. **36**, 47 (2002).
[10] P. Satir and S. T. Christensen, Ann. Rev. Physiol. **69**, 377 (2007).
[11] R. B. Bird, R. C. Armstrong, and O. Hassager, *Dynamics of Polymeric Liquids. Fluid mechanics* (John Wiley & Sons, New York, 1977), Vol. 1.
[12] E. Lauga, Phys. Fluids **19**, 083104 (2007).
[13] J. Happel and H. Brenner, *Low Reynolds Number Hydrodynamics* (Prentice-Hall, Englewood Cliffs, NJ, 1965).
[14] G. R. Fulford, D. F. Katz, and R. L. Powell, Biorheology **35**, 295 (1998).
[15] C. Brokaw, J. Exp. Biol. **55**, 289 (1971).
[16] S. Camalet, F. Jülicher, and J. Prost, Phys. Rev. Lett. **82**, 1590 (1999).
[17] K. E. Machin, J. Exp. Biol. **35**, 796 (1958).
[18] C. H. Wiggins and R. E. Goldstein, Phys. Rev. Lett. **80**, 3879 (1998).
[19] L. D. Landau and E. M. Lifshitz, *Theory of Elasticity* (Pergamon, Oxford, 1986), 3rd ed.
[20] P. Y. Tam, D. F. Katz, and S. A. Berger, Biorheology **17**, 465 (1980).
[21] E. Lauga, Phys. Rev. E **75**, 041916 (2007).
[22] See EPAPS Document No. E-PRLTAO-99-067750 for animations displaying the beating pattern for one of the eight plots shown in Fig. 2. For more information on EPAPS, see http://www.aip.org/pubservs/epaps.html.
[23] R. Dreyfus, J. Baudry, M. L. Rober, M. Fermigier, H. A. Stone, and J. Bibette, Nature (London) **437**, 862 (2005).